Bioconjugate Chemistry

Article

Cite This: Bioconjugate Chem. 2019, 30, 2060−2074

pubs.acs.org/bc

Nanoparticle Size Influences Localized Enzymatic Enhancement—A Case Study with Phosphotriesterase

Joyce C. Breger,[†,#] Eunkeu Oh,[‡,∥,#] Kimihiro Susumu,[‡,∥] William P. Klein,[†,⊥] Scott A. Walper,[†] Mario G. Ancona,[§] and Igor L. Medintz*[,†]

[†]Center for Bio/Molecular Science and Engineering, Code 6900, U.S. Naval Research Laboratory, Washington, D.C. 20375, United States

[‡]Optical Sciences Division, Code 5600, U.S. Naval Research Laboratory, Washington, D.C. 20375, United States

[§]Electronics Science and Technology Division, Code 6800, U.S. Naval Research Laboratory, Washington, D.C. 20375, United States

[∥]KeyW Corporation, Hanover, Maryland 21076, United States

[⊥]National Research Council, Washington, D.C. 20001, United States

Supporting Information

ABSTRACT: Enhancements in enzymatic catalytic activity are frequently observed when an enzyme is displayed on a nanoparticle (NP) surface. The exact mechanisms of how this unique interfacial environment gives rise to this phenomenon are still not understood, although evidence suggests that it can help alleviate some of the enzyme's rate-limiting mechanistic steps. The physicochemical limitations that govern when this process arises are also not known including, in particular, the range of NP size and curvature that are associated with it. To investigate the latter, we undertook a case study using the enzyme phosphotriesterase (PTE) and a series of differentially sized gold NPs (AuNPs). PTE, expressed with a terminal hexahistidine sequence, was ratiometrically coordinated to a series of increasing size AuNPs (diameter ≃ 1.5, 5, 10, 20, 55, 100 nm) surface-functionalized with Ni^{2+}-nitrilotriacetic acid ligands and its activity assayed in a comparative format versus that of equivalent amounts of free enzyme controls. PTE-AuNP samples were prepared where the total PTE concentration and NP surface density were kept fixed by varying AuNP concentration along with the converse format. Assembly to the AuNPs increased PTE k_{cat} ca. 3−10-fold depending upon NP size, with the smaller-sized particles showing the highest increase, while enzyme efficiency only increased 2-fold. Further kinetic testing suggested that the PTE enhancement again arose from alleviating its rate limiting step of enzyme−product release and not from a change in the activation energy. Comparison of k_{cat} and enzyme specificity with AuNP diameter revealed that enhancement was directly correlated to AuNP size and curvature with the smaller NPs showing the largest kinetic enhancements. Kinetic simulations showed that almost all of the PTE enhancement variation across AuNP sizes could be reproduced by adjusting only the rate of enzyme−product dissociation. Understanding how NP size directly affects the enhancement of an attached enzyme can provide a rational basis for designing hybrid enzyme−NP materials that specifically exploit this emergent property.

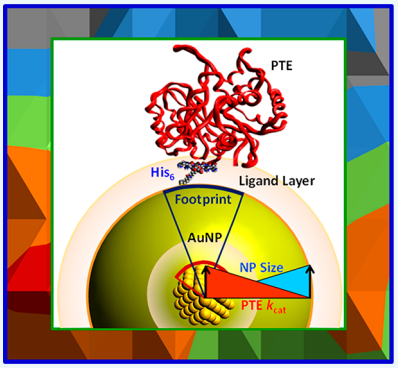

Downloaded via US NAVAL RESEARCH LABORATORY on April 21, 2020 at 12:06:58 (UTC).
See https://pubs.acs.org/sharingguidelines for options on how to legitimately share published articles.

INTRODUCTION

The advent of synthetic biology is directly predicated on the power of enzymes to achieve all the necessary chemoselective transformations for implementing both established and de novo synthetic biochemical pathways.[1−4] Most of the current efforts are focused on so-called "chassis" design which seeks to produce bacterial strains that are amenable to the repetitive large scale metabolic engineering required for creating living cell-based factories which host designer synthetic pathways to produce targeted (bio)chemicals.[5−7] However, such cell-based approaches are not without many significant challenges including ubiquitous toxicity issues and the need to efficiently transport sat I ubstrate in and product out of cells through the cell membranes. An alternative technology that has equal potential but is much less explored is that of cell-free synthetic biology.[2,8−11] In its most reductionist form, cell-free synthetic biology only requires the substrates, cofactors, and enzymes from a given pathway to achieve a targeted synthesis; this is sometimes referred to as synthetic biochemistry.[12] The issue then becomes one of stabilizing a given enzyme's structure and function for long-term activity and finding ways to overcome diffusion limitations between multiple participating enzymes so as to achieve high efficiency and high rates of sustained catalytic flux.[13] In this vein, many types of biotic and abiotic scaffolding materials from designer DNA origami and recombinant virions to molecular organic frameworks (MOFs) are currently being researched for their ability to stabilize attached enzymes while also colocalizing them for

Received: May 21, 2019
Revised: June 20, 2019
Published: July 8, 2019

© 2019 American Chemical Society

DOI: 10.1021/acs.bioconjchem.9b00362
Bioconjugate Chem. 2019, 30, 2060−2074

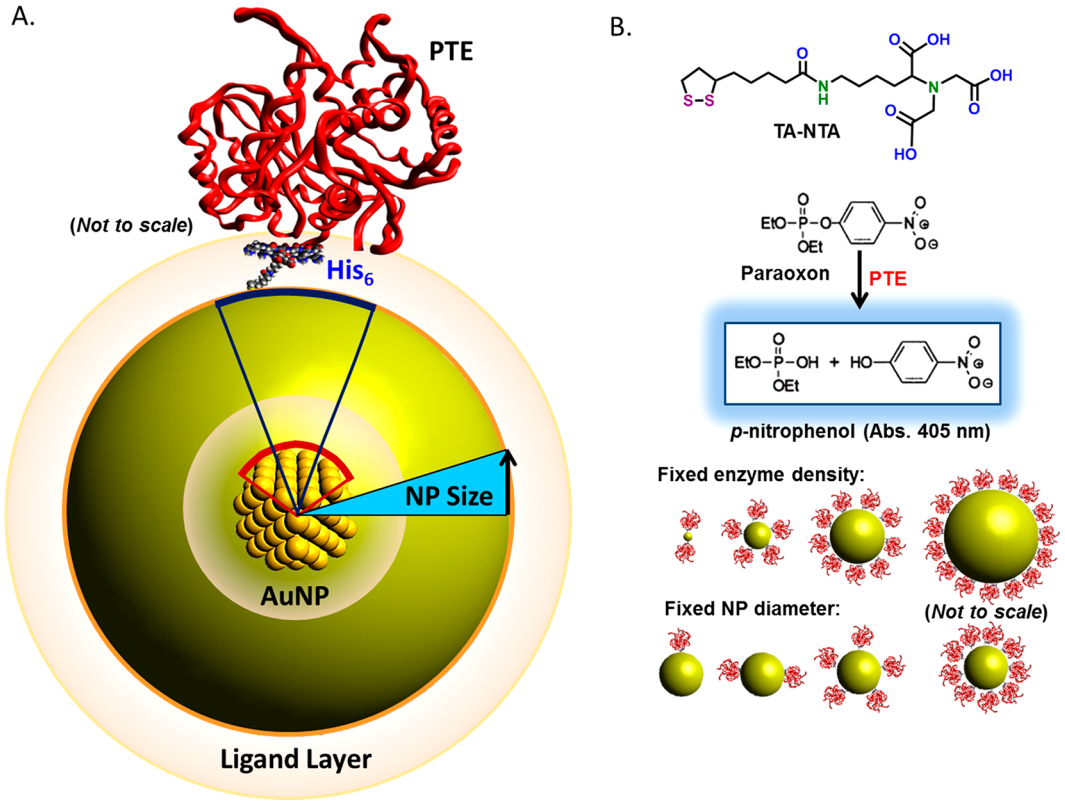

Figure 1. AuNP-PTE conjugation, ligand structure, paraoxon hydrolysis, and experimental format. (A) Schematic of the PTE monomer assembly to series of NTA-functionalized AuNPs of different sizes ranging from small 1.6-nm-diameter Au clusters (AuNC, as depicted by the center gold atoms) to large ∼100-nm-diameter AuNPs as depicted by the entire gold sphere. The schematic highlights the differences in surface area that an enzyme will occupy due to changes in NP curvature and size even though the enzyme's footprint remains the same as depicted by the red arc. There is more surface space on the larger NPs for the enzyme to attach and move around compared to that of the smaller AuNPs. The hydrodynamic diameter (H_D) of free PTE is ∼4.4 nm while the H_D of the NPs is increased by ∼6 nm following PTE assembly. (B) Top, structure of the TA-NTA ligand used to make the AuNP series colloidally stable and coordinate the PTE following Ni^{2+} loading by the NTA. Middle, conversion of paraoxon substrate in *p*-nitrophenol product by PTE catalysis. Bottom, schematic highlighting the two different experimental formats utilized in these studies. A fixed enzyme density keeps the coverage per unit area of the NP constant across the NP size series while the fixed NP diameter varies the number of enzymes per NP while keeping the NP size constant. Note, both formats keep enzyme concentration constant.

efficient biosynthesis and other purposes such as biosensing.[9,13−17] Among this diverse set of materials, it has recently become evident that nanoparticles (NPs), in particular, may have much to offer as a scaffold for hosting minimal cell-free synthetic biochemistry.

A growing body of literature has repeatedly confirmed that not only can enzymes be stabilized for long-term application by attachment to NPs, but in many cases their catalytic properties are also significantly enhanced.[18−23] Some representative examples include ∼4-fold increases in initial rates for gluconases displayed on 5−10-nm-diameter semiconductor quantum dots (QDs),[24] 4-fold increases in k_{cat} for *β*-galactosidase on 4−9 nm QDs,[25] 30% drops in activation energy for cholesterol oxidase on 10−56 nm Fe_3O_4 NPs,[26] and >1000-fold improvements in pepsin affinity (K_M) on 30 nm gold NPs (AuNPs).[27] This enhancment phenomenon does not appear to be linked to any particular enzyme type, reaction type, enzyme size, or NP scaffold material. There is, however, some evidence that the NP-enzyme bioconjugation chemistry used to create the hybrid structure is important with homogeneous and oriented enzyme displays on NPs being more often associated with the enhancement phenomena; see refs 18−21,28−31 and therein.

Using horseradish peroxidase displayed on QDs and coupled to free glucose oxidase, Vranish and co-workers demonstrated that enzyme enhancement can be maintained and can improve coupled enzymatic activity even when the second enzyme is freely diffusing in solution.[32] Vranish et al. also recently showed that attaching lactate dehydrogenase (LDH) to ∼4.3-nm-diameter QDs and to ∼10 × 4.5 × 0.4 nm rodlike QDs also provided significant enhancement in LDH activity by >50-fold.[33] More importantly, when LDH was functionally paired with pyruvate kinase (PykA) on the QD surface, their coupled activity was also magnified by >100-fold over that of freely diffusing enzyme controls. Experimental data and kinetic simulations provided strong evidence that this enhancement was a result of substrate channeling between the enzymes. In contrast to this, when Mukai et al. tethered 10 sequentially functional glycolytic enzymes to 500-nm-diameter silica particles, they did not observe individual enzymatic enhancements nor any channeling-like behavior, and indeed the catalytic properties of the enzymes appeared to be even weakened.[34] Although there are many variables associated with NPs in these applications (e.g., material type, surface chemistry, enzyme attachment chemistry, experimental buffer), it is apparent from these and some similar studies[18−21] that NP size, and its directly correlated properties of surface area and curvature, are probably important contributing parameters to enzyme enhancement on NPs, and quite likely also for

DOI: 10.1021/acs.bioconjchem.9b00362
Bioconjugate Chem. 2019, 30, 2060−2074

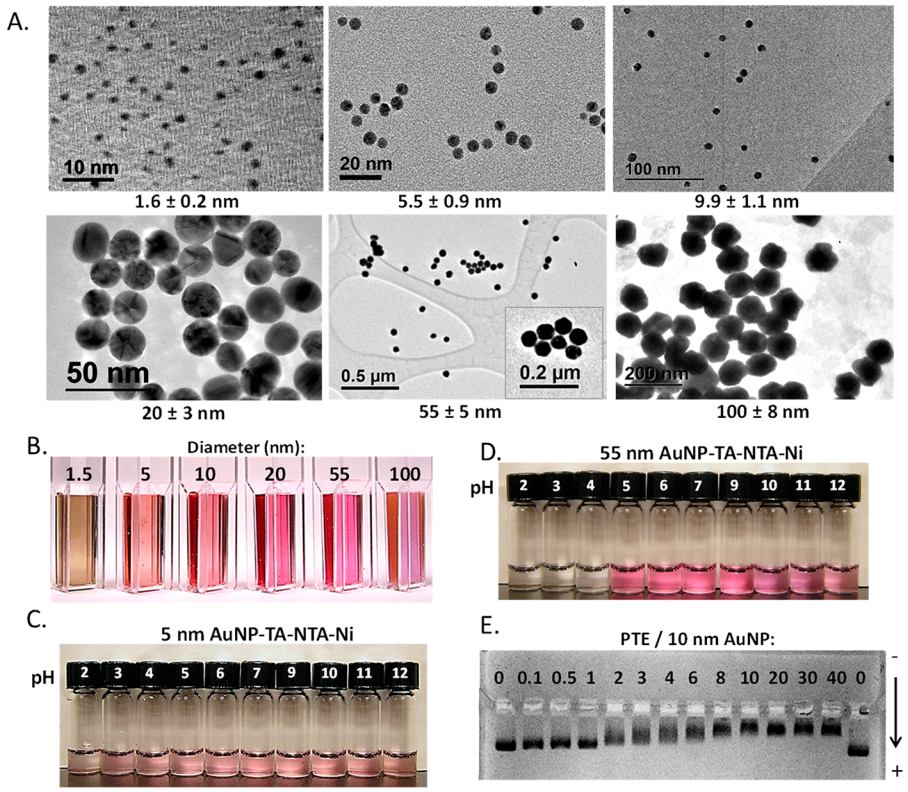

Figure 2. Selected characteristics of the AuNP series. (A) Representative TEM images of the as-synthesized NTA-AuNPs along with their average sizes as estimated from analysis of more than 100 structures per sample. (B) Photograph highlighting the different colors observed for each of the AuNP dispersions. Photographic images of (C) 5 nm and (D) 55 nm AuNPs with Ni^{2+}-loaded TA-NTA surface ligands after 24 h in buffer at the indicated pH. (E) Image of an agarose gel after 5 min of electrophoretic separation. Samples of the 10-nm-diameter AuNPs surface functionalized with the Ni^{2+}-metalated TA-NTA ligand and assembled with the indicated ratios of PTE. Samples contain 0.4 pmol AuNP and are separated in a 1% agarose gel buffered with 1 × TBE. AuNP migration rate slows in a manner that reflects the ratio of PTE assembled.

accessing channeling mechanisms when placing multiple enzymes in these types of composite configurations.

In order to evaluate the effects of NP size on enzymatic enhancement in a meaningful manner, it is critical to reduce the number of variables in these complex assemblies ideally to one, namely, that of NP size alone.[35] To this end, we utilize here a series of custom-synthesized AuNPs of increasing size as a nanoscaffold to evaluate NP size effects on the catalytic activity of phosphotriesterase (PTE), a well-characterized organophosphate hydrolase enzyme that has been previously shown to undergo kinetic enhancement when displayed on QDs; see Figure 1. Enhancements in QD-PTE activity (k_{cat} ~ 4× and k_{cat}/K_M ~ 2×) were attributed to an increase in the enzyme's rate-limiting step, namely, that of enzyme−product dissociation.[36] The AuNP size series utilized in the current study were surface functionalized and made colloidally stable with a nitrilotriacetic acid (NTA) modified dithiolated ligand which also provides for homogeneous and oriented immobilization of the enzyme via metal affinity coordination. The ability of the NPs to stabilize PTE's long-term activity and also enhance its kinetic properties in a size-dependent manner were then analyzed in the context of PTE reaction dynamics. Numerical simulations of the kinetic data provide strong evidence that the enzymatic enhancement results from alleviation of PTE's rate-limiting step.

RESULTS

Synthesis of the AuNP Size Series, PTE, and PTE Conjugation to AuNPs. A full description of the Materials and Methods can be found at the end of the document; see also the Supporting Information (SI) for further experimental details. The smaller 1.5-, 5-, and 10-nm-diameter AuNP size series were synthesized directly in water with 50:50 thioctic acid:nitrilotriacetic acid modified thioctic acid (TA:TA-NTA) ligands as described in the Materials and Methods section. The larger 20-, 55-, and 100-nm-diameter AuNPs were synthesized using a seeded growth method with citrate and ascorbic acid as coordinating ligands and then underwent further surface ligand exchange with the 50:50 ligand mixture to display the TA and TA-NTA ligands (Figure 1B-top). From this we assume that the AuNP size series continues to maintain the same display ratio of ligand. This would allow a fitting maxima of ~16 TA-NTA ligands on the smallest 1.5 nm AuNPs which is more than sufficient for the experiments described below.[37] The number of TA-NTA ligands on the larger AuNPs scales by size and is obviously far larger and also more than sufficient for the protein ratios described below.[38] TEM analysis of multiple samples confirmed the average sizes of the AuNP-NTA series, as shown in Figure 2A, where the variation in size was found to be in the range of 8−15% depending upon the particular sample. Averaged diameters as measured by TEM were found to be 1.6 ± 0.2 nm for the nominal 1.5 nm AuNPs, 5.5 ± 0.9 nm for the 5 nm AuNPs, 9.9 ± 1.1 nm for the 10 nm AuNPs, 20 ± 3 nm for 20 nm AuNPs, 55 ± 5 nm for the 55 nm AuNPs, and 100 ± 8 nm for the 100 nm AuNPs (Figure 2). Despite slight differences from the expected sizes, we refer to the AuNPs by their nominal diameters for simplicity in the rest of the text. We note that the 1.5 nm materials are not

DOI: 10.1021/acs.bioconjchem.9b00362
Bioconjugate Chem. 2019, 30, 2060−2074

technically NPs per se, but are more correctly characterized as Au nanoclusters (AuNC) which are also known for their complex photoluminescence (PL) properties.[37,39−42] UV−visible spectroscopy showed that the AuNPs had the typical and distinctive surface plasmon resonance bands (SPB) between 500 and 570 nm depending upon their size except for the 1.5 nm materials, which were featureless; see SI Figure S1. These results are quite similar to those for analogous AuNPs that were similarly synthesized or cap-exchanged with a variety of other surface ligands in our previous work.[38−40,43−45]

The AuNP-NTA series was next activated with $NiCl_2$ using column chromatography as described in the Materials and Methods. These samples kept their distinctive colloidal colors (i.e., absorption color from the front and a different color from the side of the cuvette especially for larger AuNP sizes with stronger scattering characteristics) following Ni^{2+} loading; see Figure 2B. This indicated that the AuNP-NTA-Ni^{2+} materials did not aggregate or undergo etching or other deleterious effects. The AuNP-NTA-Ni^{2+} size series also retained their colloidal properties over a pH range of 5 to 12 over time as highlighted in the representative images shown in Figure 2C,D for the 5- and 55-nm-diameter NPs, respectively. In all subsequent experiments and text, AuNPs refer to the as-prepared AuNP-NTA-Ni^{2+} unless otherwise stipulated. For enzyme bioconjugation to the AuNPs, we again rely on direct metal affinity coordination between the enzyme's terminal hexahistidine $(His)_6$ residues and the NTA-Ni^{2+} groups displayed around the NP surface; see Figure 1A,B.[29,46−48] Similar to the metal affinity coordination of polyhistidine-appended proteins and peptides to ZnS-shelled QDs, this bioconjugation strategy allows for control over the orientation of the enzyme relative to the NP since it is site-specific, while also providing control over the average number or valence of proteins attached to each NP in a manner that follows a Poisson distribution.[29,46−48] Indeed, this same chemistry was previously utilized to assemble recombinant enzymes to other similarly functionalized AuNPs.[49]

As our model enzyme for this study we utilize the organophosphate hydrolase PTE (EC 3.1.8.1). The PTE variant used originates from *Brevundimonas diminuta* as described by Raushel, and expresses as 341 residues (MW ∼ 37 kDa) with a C-terminal hexahistidine or $(His)_6$ tag, and forms a functional obligate dimer with each subunit displaying a binuclear divalent Zn center required for the catalytic reaction.[50,51] PTE is capable of hydrolyzing organophosphate esters such as the nerve agents sarin and tabun along with the commercial insecticide paraoxon, capabilities that have made PTE of interest for bioremediation and mitigation of chemical nerve agents and for cleanup of organophosphate pesticides.[52,53] Enhancements in the activity of PTE (and of a de novo expressed PTE trimer) following NP attachment have previously been reported, hence its choice here.[36,54,55] For example, PTE display on ca. 4.2- and 9.3-nm-diameter QDs resulted in a 4-fold increase in initial catalytic rates and a 2-fold increase in efficiency (k_{cat}/K_M).[36] Similar magnitude enhancements were noted for a PTE trimer although this enzyme displayed a much lower catalytic rate that was attributed to disruption of the functional dimeric unit into 3 separate monomers.[54] For monitoring PTE activity, commercially available paraoxon was used as a substrate; see Figure 1B-middle. PTE acts on the substrate's esterified phenol group to produce a *p*-nitrophenol (pNP) product which displays a strong absorption that is monitored by its large molar extinction coefficient (∼18,000 M^{-1} cm^{-1}) at 405 nm.

Although PTE is dimeric, the ratiometric values of PTE assembled per NP utilized are based on the number of PTE units per NP in keeping with enzymatic convention unless otherwise stipulated. To confirm the robustness of the conjugation along with the ratiometric control over PTE display valence on the AuNPs, they were assembled with increasing ratios of PTE and separated in agarose gels. Figure 2E shows representative results after 5 min separation on a 1% agarose gel buffered with 1 × TBE (pH 8.3) for 10-nm-diameter AuNPs that were assembled with increasing ratios of PTE. A clear decrease in AuNP migration rate is seen that directly correlates with increasing PTE display valence, confirming the ratiometric assembly of PTE on the AuNPs. Given PTE's predicted net charge of −3 at this pH, this result reflects the fact that the added size (increased hydrodynamic diameter) that PTE is contributing to the ensemble bioconjugate is dominating the migration rate in the gel. Moreover, the ability of the conjugates to remain intact even while migrating through an agarose sieving matrix demonstrates the robustness of the PTE-AuNP conjugation. Similar gel separation experiments confirmed that the PTE robustly assembled to all of the different sizes of AuNP materials (data not shown). We also did not find any evidence of AuNP cross-linking by the 2 × $(His)_6$, as was noted with far larger tetrameric proteins having 4 × $(His)_6$ and on QDs.[33] Figure S7 shows representative TEMs of 10 nm AuNPs at both low and high ratios confirming no aggregate formation, while Figure S8 shows representative dynamic light scattering (DLS) results from the same materials which also show that no aggregates formed. Importantly, the pattern of increases in hydrodynamic size as a function of PTE ratio (Figure S8) is analogous to that seen over the same ratios for change in gel migration rate of AuNPs with PTE assembly (Figure 2E).

The dissociation constant (K_d) of the polyhistidine−NTA interaction is generally accepted to be in the ∼1−10 μM range;[56,57] however, typical assays were carried out at much lower AuNP-NTA-PTE assembly concentrations. The AuNP-NTA-PTE conjugates were demonstrated to be far more robust and remained assembled through a wide dilution range for several inter-related reasons. As an obligate dimer, each functional PTE protein is potentially coordinated to the AuNPs by two $(His)_6$-NTA-Ni^{2+} interactions which would significantly improve (i.e., lower) the estimated K_d by at least several orders of magnitude.[46,58] This same multipoint coordination to the AuNPs can also be important in stabilizing PTE over the long term (vide infra). The high avidity of NTA-Ni^{2+} groups densely packed on the NP surfaces would allow for multiple potential interactions with each pendent $(His)_6$ and for quick reassembly after any potential dissociation event. Moreover, the assemblies are further left to coordinate overnight to provide for the most stable and highest-affinity interactions. Indeed, no evidence of AuNP-NTA-PTE conjugate dissociation was noted at any of the lower concentrations used in this study. See also below for confirmation of PTE loading efficiency on the AuNP series.

Enzymatic Assays with Fixed Enzyme Density or Fixed AuNP Diameter. In designing the assays, it is important to be cognizant of the enzyme loading capacities for the various-sized AuNPs, since if upper maxima are approached one would expect steric effects to alter behavior. In the SI Table S1, we estimate approximate enzyme loading

DOI: 10.1021/acs.bioconjchem.9b00362
Bioconjugate Chem. 2019, 30, 2060−2074

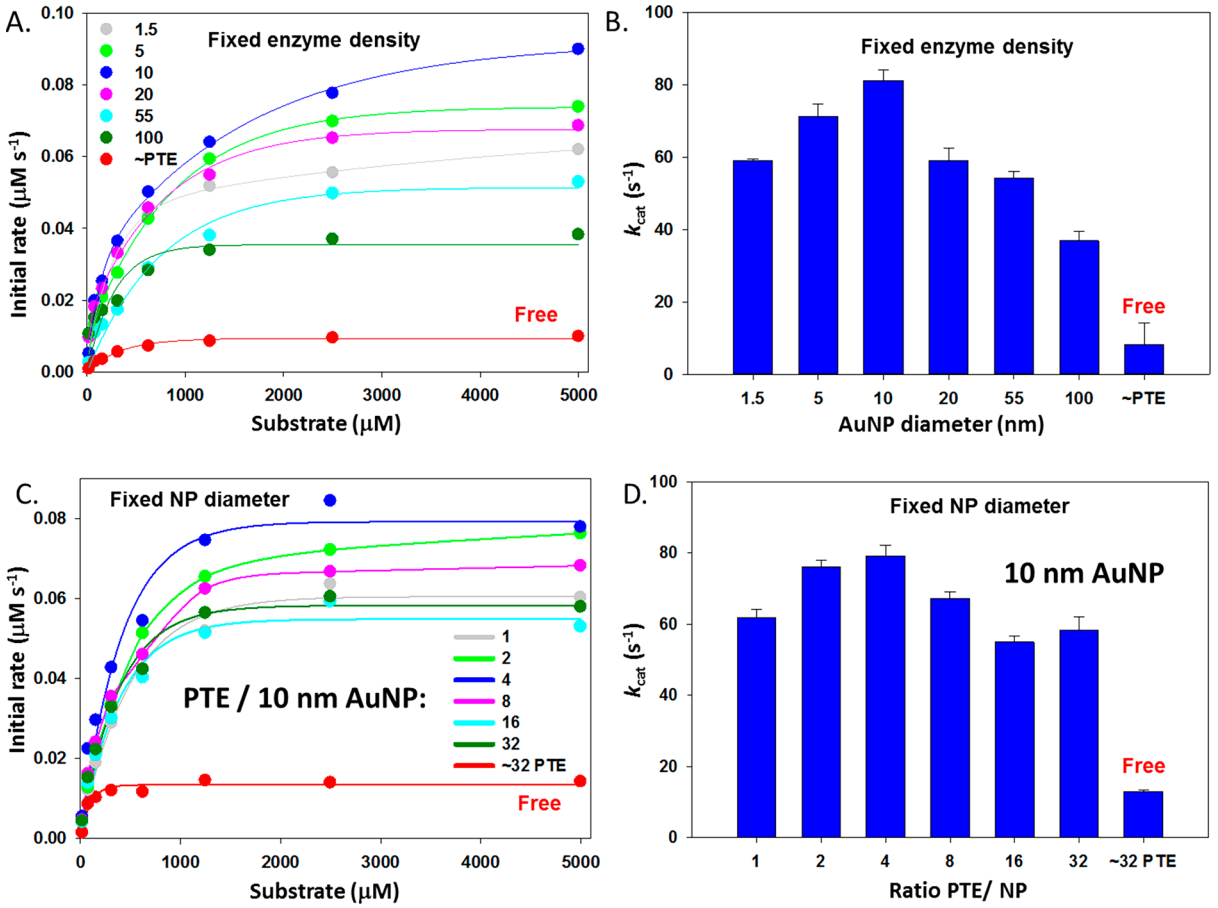

Figure 3. Fixed enzyme density versus fixed nanoparticle diameter formats. (A) Plot of representative initial rates of PTE activity on the AuNP size series using the fixed enzyme density format. Data points are shown as circles while fits are shown as lines. (B) Corresponding k_{cat} values estimated from the data. Final experimental ratios of PTE/NP utilized: 1.25 PTE/1.5 nm AuNP, 1.5/5 nm, 6/10 nm, 24/20 nm, 182/55 nm, 601/100 nm. (C) Representative initial rates of PTE activity on the 10 nm AuNPs using the fixed NP diameter format *versus* enzyme ratio along with (D) the corresponding k_{cat} values estimated from the data. Final concentration of PTE remained fixed at 1.1 nM.

Table 1. Experimentally Measured PTE Conjugation Efficiency

High coverage PTE/AuNP						
AuNP size	1.5 nm	5 nm	10 nm	20 nm	55 nm	100 nm
Reaction ratio	2.5	8	32	128	969	3202
Measured ratio	2.4 ± 0.1	7 ± 1.1	31 ± 0.5	111 ± 6.0	875 ± 65	2608 ± 230
Conjugation efficiency (%)	96.0 ± 4.1	87.5 ± 15.7	96.9 ± 1.6	86.7 ± 5.4	90.3 ± 7.4	81.4 ± 8.8
Measured deviation (%)	−4	−13	−3	−13	−10	−19
Low coverage PTE/AuNP						
AuNP size	1.5 nm	5 nm	10 nm	20 nm	55 nm	100 nm
Reaction ratio	1.25	1.5	6	24	182	601
Measured ratio	1.1 ± 0.1	1.2 ± 0.2	4 ± 1.1	18 ± 2.2	147 ± 21	392 ± 53
Conjugation efficiency (%)	88.0 ± 9.1	80 ± 16.7	66.7 ± 27.5	75.0 ± 12.2	80.8 ± 14.3	65.2 ± 13.5
Measured deviation (%)	−12	−20	−33	−25	−19	−35

capacities for the AuNPs using the size of its crystallographic structure on the available surface area and physical fitting constraints in silico in a manner similar to that described previously.[33,59] For the 10 nm AuNPs, for example, we estimate a maximum capacity ranging from 33 to 58 dimeric PTEs depending on whether the enzyme is attached horizontally by both His_6 tags or extended vertically from a single point of attachment, respectively. For the fixed AuNP size experiments, these capacities define the range over which the PTE-AuNP ratios can be varied. For the fixed enzyme density experiments, we instead select coverage values significantly less than the maximum loading so as to not incur steric issues. For example, in Figure 3A,B for the 10 nm AuNP we utilize PTE:AuNP = 6 as our low coverage value while a ratio of 32 is the high coverage value. For the other AuNPs, PTE:AuNP ratios were utilized that vary with the square of the NP radius (except for the 1.5 nm NPs) in order to keep the PTE density nominally the same with the experimental ratios summarized in the Figure 3 legend. As discussed in the SI, this scaling of ratios provides each dimeric

DOI: 10.1021/acs.bioconjchem.9b00362
Bioconjugate Chem. 2019, 30, 2060−2074

enzyme with an averaged occupation area of ~19.6 nm^2 on the surface of the 5−100-nm-diameter NPs. For the 1.5 nm NPs, the small size—which approaches that of an individual PTE—led us to use a different density, namely, 1.25 PTE/NP as a safe estimate of lower loading density. In order to make a direct comparison across equivalent samples, the actual amount of PTE in the experiments *was always kept constant* while the AuNP concentration was varied to yield the desired conjugate ratios. We also undertook experiments to confirm that PTE conjugation to the different AuNPs actually occurred efficiently across the range of both low and high coverage ratios; see Materials and Methods. This confirmed our rationale that PTE bound tightly to the AuNPs and that the ratios chosen for actual experiments were appropriate as an overall averaged attachment efficiency of 83 ± 10% was achieved; see Table 1. The 10 nm AuNPs achieved the highest efficiency attachment for high coverage at ~97%, while 100 nm NPs only attained ~65% at low coverage.

Figure 3A presents a set of representative plots showing the initial rates of paraoxon-to-pNP conversion by PTE assembled on the AuNP size series with fixed enzyme density as compared to free PTE. Also shown in the plots are the Michaelis−Menten (MM) curve fits obtained by fitting eq 3(i) with k_{cat} and K_M being the regression parameters; the values are listed in Table 2. Figure 3B shows a histogram of the average k_{cat} values, and for all NPs we find them substantially increased over that for free PTE of ~8.2 s^{-1}, shown as the rightmost bar in Figure 3B. This ranges from a 4.5-fold increase for the 100 nm NPs up to ~10-fold for the 10 nm AuNPs. For comparison, we note that PTE activity was enhanced at most 4-fold when assembled to 4.3-nm-diameter QDs.[36] Other relevant kinetic descriptors obtained for the fixed enzyme density experiments, including average values for K_M and k_{cat}/K_M, are listed in Table 2. The K_M values all increased ~3−10-fold (decreased affinity), with the largest changes corresponding to the AuNPs that showed the largest increases in k_{cat}. This is expected since k_{cat} and K_M are functionally correlated unless the enzyme's activity undergoes a more complex mechanistic change to its catalytic process-(es).[60] Enzyme efficiency, as measured by the second-order rate constant k_{cat}/K_M, also increased up to 2-fold primarily for the smaller NPs, as also occurred previously with QDs.[36] Control experiments confirmed that the AuNPs did not catalyze paraoxon hydrolysis on their own (data not shown).

Table 2. Averaged Enzyme Activities for Fixed Enzyme Density Format for Low Coverage Conditions[a]

AuNP size	k_{cat} (s^{-1})	K_M (μM)	k_{cat}/K_M (mM^{-1} s^{-1})
1.5 nm	59.1 ± 0.4	222 ± 24	265 ± 104
5 nm	71.3 ± 3.3	583 ± 86	122 ± 19
10 nm	81.2 ± 3.0	443 ± 56	187 ± 18
20 nm	59.0 ± 3.4	328 ± 69	186 ± 14
55 nm	54.3 ± 1.8	655 ± 66	82 ± 9
100 nm	36.9 ± 2.5	198 ± 43	190 ± 28
PTE	8.2 ± 6.0	67 ± 15	130 ± 2

[a]Taken from Figure 3A,B.

In our experiments with the fixed NP diameter and varied PTE coverages, the total enzyme concentration was always kept fixed and the AuNP concentration was adjusted to achieve the various PTE:AuNP ratios for each given AuNP size. The 10 nm AuNP series is highlighted in Figure 3C,D and in this case the PTE:AuNP ratios ranged from 1 to 32 monomeric enzymes per NP, which represents approximately 3% to 89% of the estimated lower maximum capacity surface fitting range. Figure 3C presents the initial PTE rates for the 10 nm AuNPs at the indicated assembly ratios along with the analogous curve for free PTE. The rate plots all saturate in the 0.05−0.08 μM s^{-1} range of turnover which is ~5−8-fold that of the free enzyme at the highest concentration. Figure 3D shows a histogram of the k_{cat} values extracted from these data with the corresponding K_M and k_{cat}/K_M descriptors given in Table 3. The highest and lowest k_{cat} values were 79.2 and 55.0 s^{-1} for ratios of 4 and 16 PTE/NP, respectively, with the average value being ~66.3 ± 9.7 s^{-1}. This represents an enhancement range of 4- to 6-fold over that of free PTE. The K_M was again directly increased by 4 to 6× (lower affinity) while the efficiency (k_{cat}/K_M) only increased by ~1.7× at most for the ratio of 4. Data from testing the other AuNPs in the size series in a similar manner are provided in the SI.

PTE Stabilization by AuNP Conjugation and Subsequent Activity. In the course of performing the foregoing experiments, we noticed a slight decrease in the catalytic activity of the control free PTE samples over time. In previous studies with LDH,[33] it was determined that the free LDH tetramer underwent a cooperative dissociation process as its concentration was diluted with an estimated apparent dissociation constant K_D^{app} of ~12 nM and this led to inactivation. In contrast, LDH attachment to the QDs by its four terminal polyhistidine sequences resulted in significant enhancement of activity presumably by stabilizing the quaternary structure of the tetramer as QD−enzyme conjugate concentration was lowered over the same range. PTE stability over time was not something explicitly considered in previous analyses of PTE activity as assembled to QDs or other NPs.[36,49]

Preliminary measurements of PTE specific activity when serially diluted showed no evidence of dissociation for either the free enzyme or when attached to 5 nm AuNPs (data not shown). Figure 4A plots representative data where the same concentration of PTE was left free or displayed on 5 nm

Table 3. Averaged Enzyme Activities for Fixed NP Diameter Format on 10 nm AuNPs

PTE/NP	% NP surface coverage	k_{cat} (s^{-1})	K_M (μM)	k_{cat}/K_M (mM^{-1} s^{-1})
1	3	61.9 ± 6.6	282 ± 65	260 ± 20
2	6	76.1 ± 3.6	318 ± 22	274 ± 16
4	11	79.2 ± 3.6	304 ± 34	299 ± 33
8	22	67.2 ± 6.8	328 ± 65	254 ± 49
16	44	55.0 ± 2.1	297 ± 24	185 ± 76
32	89	58.4 ± 3.7	286 ± 47	220 ± 16
~PTE	–	13.0 ± 5.0	72 ± 55	181 ± 72

DOI: 10.1021/acs.bioconjchem.9b00362
Bioconjugate Chem. 2019, 30, 2060−2074

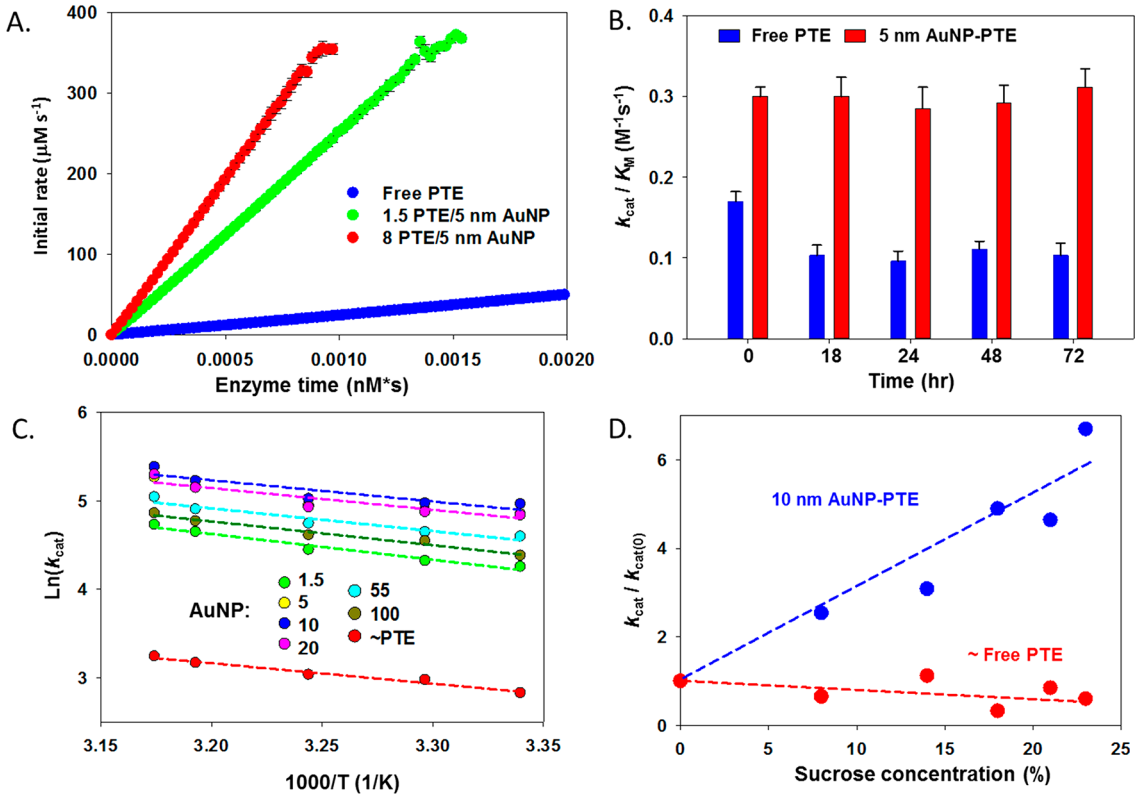

Figure 4. PTE activity, recovery of activity, and activation energy. (A) Comparison of PTE activity progress curves shown in enzyme time for free PTE and PTE assembled to 5 nm AuNP at a ratio of either 1.5 or 8 enzyme/NP. AuNP concentration was varied to achieve the ratios while PTE concentration remained constant. (B) Monitoring of PTE activity over time when left free and as assembled to 5 nm AuNPs after the time elapsed. (C) Arrhenius plot of averaged ln k_{cat} values versus inverse temperature (Kelvin) for AuNP-PTE assemblies across the AuNP size series and free enzyme. The average value of the slopes for the fitted data corresponding to the AuNP size series was -2.55 ± 0.22 versus -2.45 for the free PTE. This corresponds to an averaged activation energy of 21.7 ± 1.5 kJ mol^{-1} for the AuNPs versus 19.5 kJ mol^{-1} for the free PTE. Ratios of PTE per NP as in Figure 3A. (D) Plot showing representative experimental results of normalized PTE k_{cat} values from 1.5 nm AuNP-PTE conjugates (blue) and equivalent amounts of free PTE red assayed in the presence of increasing sucrose concentrations. Linear fits added to each data series.

AuNPs at a ratio of either 1.5 or 8 enzyme/NP; AuNP concentration was again varied to achieve the latter ratios. This plot shows the initial rate of enzyme activity as a function of enzyme time where enzyme concentration is multiplied by time ($[E] \times t$). Plots of this format are sometimes used for "Selwyn's test" and may indicate whether an enzyme is being inactivated in a given configuration.[60,61] Similar to the data in Figure 3, this plot confirms that PTE is instead being significantly activated when assembled to the AuNPs. Conversely, this data reflects a substantial reduction in PTE activity when it is not displayed on the NP. PTE activity was then monitored when an aliquot of stock free enzyme was removed from the freezer, thawed, and left in the refrigerator for increasing lengths of time. At the end of these time periods, the enzyme was assembled to 5 nm AuNPs and assayed for comparison to the activity of unassembled identically treated equivalent control PTE from the same aliquot source. Figure 4B shows the results of this comparison in terms of the enzyme's efficiency (k_{cat}/K_M) before and after NP assembly. We observe that the free enzyme does indeed lose some activity and efficiency with time when diluted from stock dropping ca. 40% from 0.17 ± 0.01 M^{-1} s^{-1} to 0.10 ± 0.01 M^{-1} s^{-1}. Similarly, our experiments, in agreement with previous work,[36] find that fresh PTE has $k_{cat} \approx 45$ s^{-1} whereas PTE kept for 24 h in solution at 1 nM drops to the level reported here. Interestingly, Figure 4B also shows that when this "aged" enzyme is assembled onto the AuNPs, it recovers its fully enhanced initial activity with a now almost unchanged averaged value of 0.30 ± 0.01 M^{-1} s^{-1}. The PTE monomer (Protein Data Bank entry 1I0D, www.rcsb.org) is predicted to express with at least two cysteine residues, and intramolecular disulfide bridges in the dimer may keep the monomer from functionally dissociating even though activity is diminished. Since it is not clear if the enzyme fully dissociates when not on the AuNPs, we associate the enhanced activity of Figure 4A and recovery of high efficiency in Figure 4B with *stabilization* of activity (and not structure) when displayed on the AuNPs.

We next performed an Arrhenius analysis to see if any change in AuNP size (and curvature) would alter the PTE activity by lowering its activation energy.[33,60] As shown in Figure 4C, the averaged slope values for the AuNP size series was -2.55 ± 0.22 versus -2.45 ± 0.18 for the free PTE, suggesting that there is no significant difference in enzyme activation energy imparted by AuNP attachment nor NP size; the estimated activation energy (E_a) values extrapolated from this data for each AuNP at both low and high coverage can be found in SI Table S2. As mentioned previously, PTE's native rate-limiting step is that of enzyme−product release (k_2 in eq 3), and detailed studies showed that PTE enhancement by QD attachment was as a result of alleviating this limiting step.[36] This was accomplished experimentally by challenging the enzyme's ability to release product with the addition of increasing sucrose concentrations to the reaction buffer. For free PTE, it was found that k_{cat} decreased with increasing

DOI: 10.1021/acs.bioconjchem.9b00362
Bioconjugate Chem. 2019, 30, 2060−2074

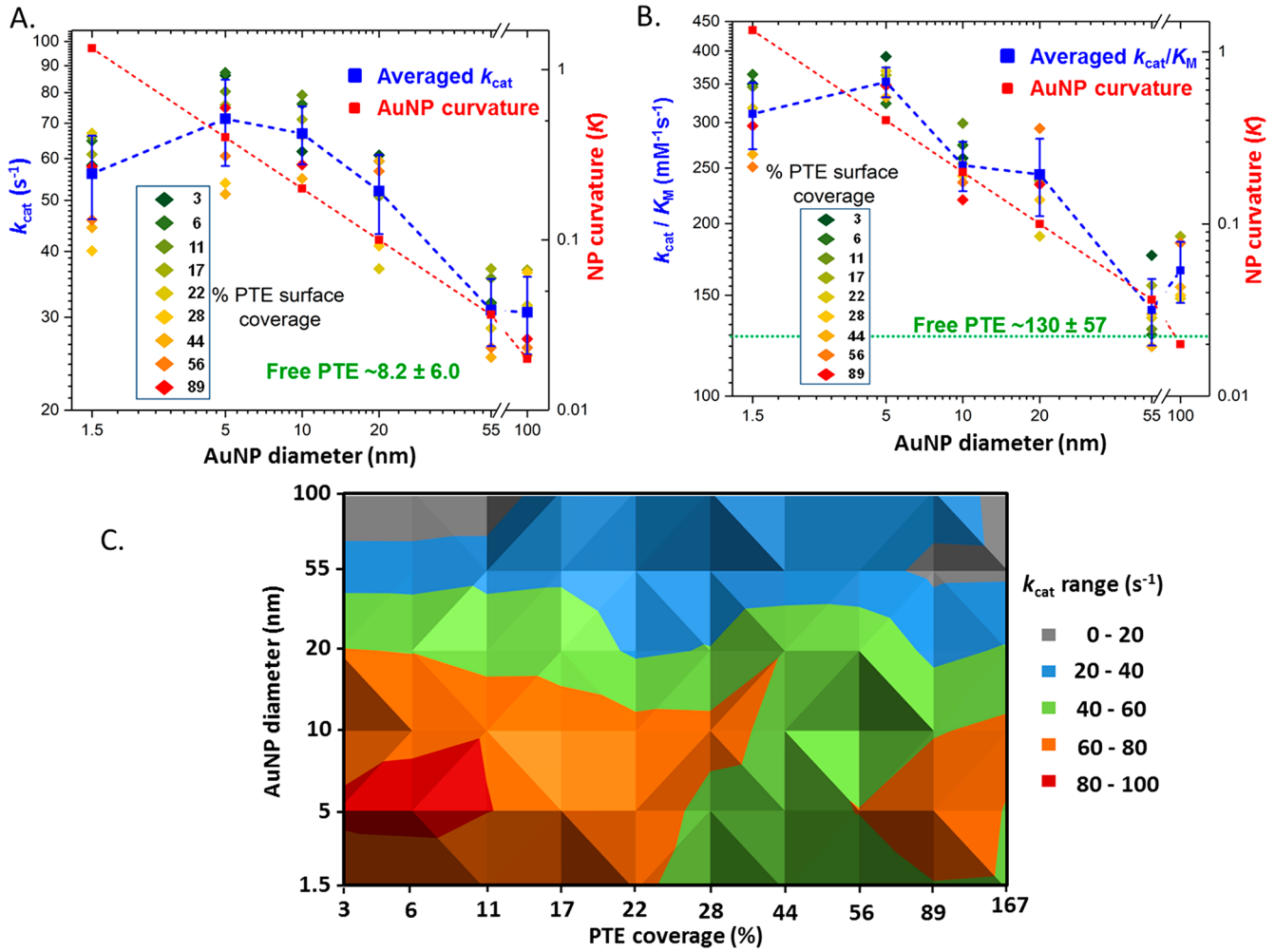

Figure 5. Averaged k_{cat} and enzyme efficiency versus PTE surface coverage and NP size. (A) Comparison of averaged PTE k_{cat} values as AuNP surface coverage increases for the AuNP size series following the indicated color coding (inset). Standard deviations for each individual points not shown for simplicity (values in SI). The average value (of individual replicates) is shown in blue along with its standard deviation. The dashed blue line joins the average values together. Unassembled free PTE k_{cat} value (8.2 ± 6.0 s^{-1}) indicated in green. AuNP curvature (κ = 1/radius) values in log scale are plotted in red with a line of best fit. (B) Comparison of averaged PTE k_{cat}/K_M values as AuNP surface coverage increases for the AuNP size series following the indicated color coding (inset). Average value is shown in blue along with its standard deviation. The dashed blue line joins the average values together. Unassembled free PTE k_{cat}/K_M value (130 ± 57 mM^{-1} s^{-1}) indicated in green. AuNP curvature (κ = 1/radius) values in log scale are plotted in red with a line of best fit. Percent PTE coverage was based on ratios of 2.5, 8, 32, 128, 969, and 3202 PTE being assembled to the 1.5-, 5-, 10-, 20-, 55-, and 100-nm-diameter NPs as the 100% coverage maxima. (C) Plot of binned k_{cat} value ranges as a function of AuNP diameter and %PTE coverage in a topographical format. Note values for the 100 nm AuNPs at lowest coverage were not collected and are extrapolated here. Values are tabulated in Table S3.

sucrose suggested that the sucrose's increase in the viscosity surrounding the enzyme made it harder for the enzyme to release product.[51,62] In contrast, the sucrose effect on QD-PTE was reversed with k_{cat} instead of increasing, showing that product release was becoming easier, perhaps as a result of higher product solubility, and suggesting that this was the reason conjugating PTE to a QD enhanced its turnover.[36] A similar series of experiments was performed here as shown in Figure 4D where normalized k_{cat} results for free PTE and for the same concentration of PTE assembled on 10 nm AuNPs at a low display coverage (as done for Figure 3B) are compared across the range of sucrose concentration. As before, the free PTE k_{cat} drops slightly in the presence of the increased sucrose, and as seen with QDs, PTE assembled on the 10 nm AuNPs instead rises. Interestingly, the increase for AuNP-mounted PTE is substantially larger than that seen for QD-displayed PTE, with the former increasing by 6-fold over the range of sucrose concentrations, whereas the latter was only ~30%.[36] Similar results were obtained for all the other AuNP sizes (SI) where the relative magnitude of the normalized k_{cat} increase on the AuNPs as a function of increased sucrose loosely tracked the enhancement pattern shown in Figure 3B. Overall, this confirmed that PTE enhancement on the AuNP size series is again associated with a rise in the rate of product release (k_2).

PTE Surface Coverage and Kinetics versus AuNP Size. As an aid to interpreting the complex effects of AuNP diameter and curvature on PTE catalytic rate and efficiency, all of the k_{cat} and k_{cat}/K_M data were replotted in log–log plots as shown in Figure 5A,B using the values listed from Table S3. The abscissae in each plot are the AuNP diameter, and different-colored symbols are used to denote the data collected across the estimated enzyme surface coverage ranging from 3% up to 89%. It is readily apparent from Figure 5A that within the data for each NP size the higher k_{cat} values are consistently seen

DOI: 10.1021/acs.bioconjchem.9b00362
Bioconjugate Chem. 2019, 30, 2060–2074

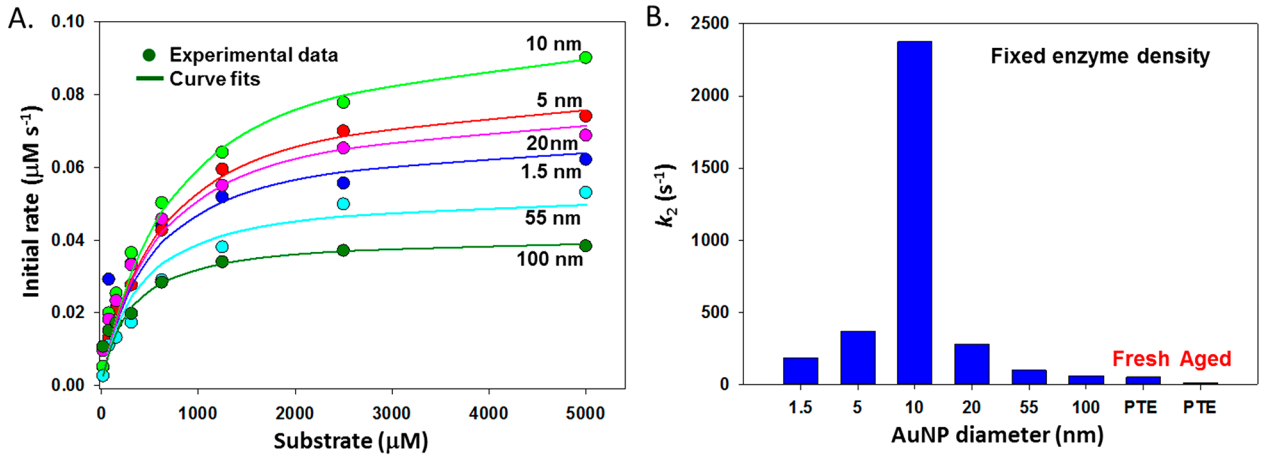

Figure 6. Curve fitting to initial rate data. (A) Curve fits in red to the experimental initial rate of PTE activity on the AuNP size series using the fixed enzyme density format taken from Figure 3A along with the extrapolated k_{cat} and K_M values k_2. (B) Values of k_2 derived from the fits in panel (A) as a function of NP diameter. A closeup of all the values below 500 s^{-1} can be found in SI Figure S9. The closeness of the two k_{cat} values in eq 5 may result in k_2 being overestimated for the 10 nm AuNPs. Low coverage format for both plots with high coverage data found in Table 4.

Table 4. Estimated k_2, $\hat{k}_{cat}$, and $\hat{K}_m$ Kinetic Values Based on Fitting Based on Fixing $k_{cat}/K_M \sim 130$ mM^{-1} s^{-1} as in Figure 6A[a]

	High Ratio[b]				Low Ratio[c]			
AuNP Size	k_2 (s^{-1})	$\hat{k}_{cat}$ (s^{-1})	$\hat{K}_M$ (μM)	R^2	k_2 (s^{-1})	$\hat{k}_{cat}$ (s^{-1})	$\hat{K}_M$ (μM)	R^2
1.5 nm	161	60.1	463	0.99	185	63.1	485	0.93
5 nm	356	75.5	581	0.99	370	76.1	585	0.99
10 nm	1852	91.1	701	0.99	2377	92.1	708	0.99
20 nm	184	63	485	0.99	279	71.3	548	0.99
55 nm	101	49.1	378	0.99	96	48.0	369	0.96
100 nm	46	31.2	240	0.90	60	37.0	284	0.97
PTE	10	9.3	268	0.99				

[a] R^2 is the regression coefficient between the experimental values and fitting curves in Figure 3. [b] High ratios correspond to ~89% surface coverage PTE/NP = 2.5, 8, 32, 128, 979, 3202 for the 1.5, 5, 10, 20, 55, 100 nm AuNPs. [c] Low ratios = 1.25, 1.5, 6, 24, 182, 601 PTE/NP for the 1.5, 5, 10, 20, 55, 100 nm AuNPs.

with lower surface coverage. The on-NP k_{cat} is always significantly higher than that of the free PTE control with the largest increase approaching 10-fold for the 5 and 10 nm AuNPs especially at lower surface coverage. The catalytic rate seen on the largest 55- and 100-nm-diameter AuNPs is not enhanced quite as much, but is still 3−4-fold above that of free PTE. For k_{cat}/K_M or enzyme efficiency (Figure 5B), the largest increase in NP enhancement is again seen with the 5 nm AuNPs which are increased 3−4-fold. The average and individual k_{cat}/K_M values for the 55 and 100 nm AuNPs are not statistically different from that of the free enzyme control.

In these same panels, plots of AuNP curvature (κ, the reciprocal of NP radius) serve as a direct comparator for how the localized NP surface geometry is changing from highly curved to almost planar across the NP size series. Decreases in both PTE k_{cat} and k_{cat}/K_M enhancement appear to be directly correlated with the drop of NP curvature in the 5−55-nm-diameter AuNP size range as both lines closely parallel each other across these values. As NP size increases and its corresponding curvature decreases, there is a steady and correlated drop in catalytic enhancement. Although significantly enhanced, the 1.5 nm AuNPs do not manifest the same enhancement as the 5 nm materials and we attribute this to their very small size. Indeed, the 1.5 nm AuNPs are smaller than that of the enzyme itself and their lack of ability to host many surface proteins or perhaps provide enough of the critical NP interfacial environment required to significantly increase catalysis may potentially contribute to the break in the size versus enhancement trend observed when going from larger to smaller NPs (vide infra). Figure 5C shows the binned k_{cat} values as a function of AuNP diameter and percent PTE coverage in a topographical format. This serves to expand the effect of relative surface coverage and size as visible variables. This helps again visualize that the highest values are found associated with the 5 nm AuNPs at the lowest percentage coverage (highest curvature with lowest PTE density) while the lowest values are associated with the largest materials (smallest curvature).

Based on the sucrose experiments described earlier in connection with Figure 4D, we concluded that for PTE attached to AuNPs the turnover is rate-limited by product release, k_2 as defined in eq 4, as had been found previously for free PTE and PTE attached to QDs.[36,51,62] This definition of k_2 now forms the basis for the subsequent discussion. In terms of the Michaelis−Menten (MM) model discussed below, the implication is that any variation with NP diameter should come solely from k_2. It is reasonable to also assume that k_{cat}^R or K_M^R are independent of the NP diameter, and if so, then a critical test of the interpretation via eq 5(iii) is whether the ratio of experimentally derived parameters $\hat{k}_{cat}/\hat{K}_M$ are independent of the NP diameter to within experimental error. Note that the hats on $\hat{k}_{cat}$ and $\hat{K}_M$ indicate that these are actual experimental values. Illustrating this with the experimental data in Figure 3A, we fix $\hat{k}_{cat}/\hat{K}_M$ at 130 mM^{-1} s^{-1}

DOI: 10.1021/acs.bioconjchem.9b00362
Bioconjugate Chem. 2019, 30, 2060−2074

(from Table 2) for all NPs from free PTE, assuming its efficiency does not change, and then perform a one-parameter regression of the data to estimate $\hat{k}_{cat}$, and in turn estimate k_2 in a manner analogous to what was done previously in refs 32,33,36,63. The curve fit is shown in Figure 6A with values tabulated in Table 4 and its quality is essentially as good as obtained previously (Figure 3A). The quality of these fits are essentially equivalent to those obtained when using $\hat{k}_{cat}$ and $\hat{K}_M$ as the fitting parameters; see Table S4. In other words, the data conform very well to the prediction of modified MM theory that $\hat{k}_{cat}/\hat{K}_M$ should be independent of NP size.

The modified MM model further claims that the dependence of the turnover on NP size (at fixed density) should depend solely on the variation of k_2 with NP diameter. As follows from eq 5(ii), we can find this variation to within an additive constant using

$$\frac{1}{k_2(d)} = \frac{1}{\tilde{k}_{cat}(d)} - \frac{1}{k_{cat}^R} \quad (1)$$

where d is the NP diameter. To use this equation, we employ the Brønsted relation to estimate $k_{cat}^R = \exp(\beta \cdot pK_a + C) \approx 95.5$ s^{-1}.[62] The resulting product release rate $k_2(d)$ based on the average kinetic parameters given in Figure 3A and Table 2 is plotted in the histogram in Figure 6B (values in Table 4). The product release rate is seen to have a pronounced maximum for a 10 nm AuNP and then declines quickly especially for larger AuNPs. Qualitatively, this characteristic is robust; however, it should be noted that the height of the peak is sensitive to error in k_{cat}^R.

DISCUSSION AND CONCLUSIONS

The primary result of this paper is that the kinetic activity of $(His)_6$-appended PTE assembled on the surfaces of AuNPs shows a clear dependence on NP diameter. Our experiments (Figure 3A,B and Figure 5A) reveal that attachment to an AuNP increases PTE's k_{cat} by up to 10-fold depending on the NP size, with the smaller sized particles showing the highest increase and especially at the lowest PTE enzyme density (highest curvature with lowest coverage). This is reflected by the orange and red patches in the lower left corner of Figure 5C. An increase in enzyme efficiency of about 2-fold is also seen (Table 1 and Figure 5B). As demonstrated most clearly in Figure 3B, the observed k_{cat} is found to correlate directly with the diameter in experiments where the number of PTEs per unit surface area of the NP was kept fixed. In an effort to understand this behavior better, we consider various mechanisms by which this dependence might come about along with the evidence for or against each.

A first hypothesis as to why the PTE turnover depends on NP size has to do with the proximity of PTEs on the surface and how this might be affected by curvature. Specifically, a smaller radius of curvature will provide more room for a given PTE relative to its neighbors and hence might enhance turnover by opening up more pathways for product release. However, the data of Figure 3C and Figure 5A show that the degree of PTE coverage on the AuNPs (at least well short of when the loading capacity is approached) has only a minor effect on the PTE turnover rate. Further support for this conclusion is provided in Table 4 where a careful comparison based on initial rate data with low and high coverage is given. In both cases, the MM model gives excellent fits, and the coefficients $\hat{k}_{cat}$ and $\hat{K}_M$ determined for the two cases are quite similar. We therefore conclude that variations in access to PTE on the surface of NPs of varying curvature in a fixed enzyme density experiment (Figure 3A,B, Tables 2 and 4) are unlikely to explain our observation that NP size has a strong effect on PTE turnover.

An implicit assumption in the foregoing is that the PTE is singly attached to the QD by the His_6 tag at one end of the dimer, and this undoubtedly will be true for small diameter AuNPs since the length of the dimer (and thus the distance between its His_6 tags) is about 9 nm. However, as a second hypothesis, it would seem likely that for "large" radii of curvature the surface will become flat enough that both His_6 tags of a PTE dimer could attach to the same AuNP especially at lower PTE:NP ratios. Obviously if this were to occur in appreciable numbers, then the loading capacity of the NP would drop considerably, and the turnover rate would also fall for denser coverages. However, the experimental observation that the turnover seems relatively independent of coverage (e.g., see Table 3 and Table S3) and the consistently high conjugation efficiency across the NP size range (Table 1) argues against this idea as well. Also, contrary is the fact that the size of the PTE dimer suggests that the effect would not become significant until the diameters were far larger than 20 nm or more; however, the drop in turnover begins for diameters above ~10 nm. On this basis, we suggest that the effect of doubly attached PTEs is at most second-order, and as such might at most account for lower ratio conjugations having slightly higher turnover rates as seen in Table 4. This is also consistent with previous results where the largest enhancements in enzymes attached to NPs tended to be found at lower enzyme/NP ratios.[20,33,36,54,63]

A final hypothesis that could possibly explain the dependence of PTE turnover on NP size again concerns the effect of curvature on surface crowding, not of PTE but rather of the TA-NTA surface ligands. The "large" triacetic acid headgroups of NTA would seem especially susceptible to nearest-neighbor interactions. The idea would be that as the radius of curvature diminishes the turnover would rise due to the relief of ligand surface crowding. This could be a result of steric hindrance or perhaps due to a concomitant increase in the product solubility and/or diffusivity in the discrete NP hydration layer. It is also possible that product partitioning may play a role here. For example, if the dielectric constant in the localized vicinity of the NP surface is reduced close to the enzyme's active site, partitioning of the product could enhance the rate of product release. Of the three hypotheses considered, this one seems the most likely, but of course the complexity of the situation and the difficulties of molecular-scale characterization make firm conclusions nearly impossible.[35] Moreover, experimentally switching to another surface chemistry is not trivial as the PTE still requires both the presence of NTA and access to it. Much as in our earlier work with PTE on QDs,[36] the complexities of the attachment of PTE to AuNPs makes it difficult to decipher the mechanisms by which the enzyme activity is enhanced following attachment and also why AuNP size is important as demonstrated herein. With regard to the enhancement, an important factor is clearly the stabilizing effect AuNP attachment has on the PTE. Most revealing is the experiment of Figure 4B wherein the loss of free enzyme activity over time could be recovered by AuNP attachment. This suggests that AuNP coordination of PTE not only stabilizes the enzyme's activity but might well serve to maintain it in an active conformation.

DOI: 10.1021/acs.bioconjchem.9b00362
Bioconjugate Chem. 2019, 30, 2060−2074

In comparing PTE when attached to an AuNP versus when attached to a QD,[36] the degree of enhancement over free PTE is not a useful measure because of the observed strong dependence of the free PTE's activity with aging (Figure 4B) and especially at low concentrations. A better gauge is a direct comparison of the MM constants observed for PTE when attached to the NPs, and for this the peak k_{cat} for PTE on AuNPs is roughly half that on QDs while k_{cat}/K_M is approximately one-third, respectively. Two factors are potentially important here, one being again the stabilization ligands with the AuNPs using TA-NTA while the QDs used a slightly smaller more zwitterionic DHLA-CL4 molecule.[36] The differing effects these might have on the hydration layer and on product solubility and/or diffusivity could easily account for the observed differences in rate enhancement. A second difference between these two systems is the means of coordination of the PTE to the NP. In the case of the QDs,[36] the PTE was directly coordinated to the QDs ZnS shell (hard surface) so that the His_6 and a portion of the enzyme had to contact and interpenetrate with the ligand shell (soft surface); this may have constrained its ability to move freely during catalysis. For the AuNPs, the PTE coordination was instead to the extended distal end of the TA-NTA ligand (soft surface). By what mechanism this difference might affect the enzyme activity is unclear, but again it seems reasonable to suppose that it influences the hydration layer and the product solubility and/or diffusivity.

More generally, it is clear that the properties of the localized NP environment are critical to the observed enzymatic enhancements and this will probably be true for many different applications that extend beyond just enzymatic use to sensing and even theranostics.[64−66] The challenge is that at the same time this key determinant of the behavior remains poorly characterized and understood. It has been recently confirmed that colloidal NPs have the "universal" property of structuring the surrounding solvent regardless of whether it is aqueous or organic.[67] Further, this structured environment can extend to a distance equal to about twice the NP diameter. This will, in turn, lead to a variety of unique physicochemical changes in the NP's surrounding environment including pH and ion gradients, changes in density, charge effects, boundary layers, and the like.[68] Such localized environments can also contribute to partitioning of substrate or products due to localized changes in dielectric constants. Moreover, NP-enzyme hybrids are not static and will diffuse in their environment in contrast to enzymes tethered to a planar surface whose activity will tend to be dominated by a boundary layer and potential stagnation effects.[20] The localized surface on the larger AuNPs approaches the planar surface limit, and this could be important in reducing the PTE enhancement in those cases. In agreement with our current findings, the observation that smaller NPs tend to induce larger enhancements in enzyme activity has been noted for many other systems.[18−21,32,33,36,54,63,69] Indeed, a similar size dependence on activity was noted for three different enzymes assembled onto a range of similar-sized Ni-NTA AuNPs in multilayer structures.[70] In that case, no overt kinetic enhancement was observed; rather, it was just increases in activity that approached the level of free untethered enzymes.

It is evident that much more work is still needed to understand the enzymatic enhancements induced by NP display. Experiments are currently in planning to vary the AuNP surface ligand character and their relative density to probe the NP surface effects, hydration layer, and the product solubility and/or diffusivity. As supported by the research presented here, the two main mechanisms for this enhancement are the impact the NP-attachment has on enzyme stability and on product release via the effect on the hydration layer and the product solubility and/or diffusivity. Another important factor to note is that, although not universal, enzyme−product release is a common rate-limiting step for many enzymes.[60] On the stability side, a dramatic example was obtained in recent work that found LDH activity to be greatly enhanced (ca. 100-fold) following attachment to a QD surface due to the stabilization of LDH's quaternary structure.[33] Finally, the advantages of a NP as a scaffold for enzymatic activity may be beneficially compounded by the fact that this approach lends itself well to enzymatic cascades wherein a sequence of multiple enzymes can be made highly efficient through mechanisms such as colocation and channeling.[33,71−73]

MATERIALS AND METHODS

Synthesis and Preparation of Gold Nanoparticles. *Direct Synthesis of 1.5−10 nm AuNPs with TA-NTA.* Synthesis of the nitrilotriacetic acid modified thioctic acid (TA-NTA, disulfide ring in close form) solubilizing ligand was as previously described.[74]AuNPs stabilized with this ligand (AuNP-TA-NTA) and with diameters of 1.5 to 10 nm were synthesized following published procedures with some modifications.[40,45] For 1.5 nm AuNPs, 100 μL (1.0×10^{-5} mol) of 100 mM tetrachloroauric (III) acid ($HAuCl_4 \cdot 3H_2O$) aqueous stock solution, 500 μL (5.0×10^{-5} mol) of 100 mM of equal mixture of TA-NTA and thioctic acid (TA) ligand stock solution, and 100 μL (2.0×10^{-4} mol) of 2 M NaOH were dissolved in 50 mL of deionized H_2O; the mixture was then stirred at room temperature for 5 min. 100 μL (1.0×10^{-4} mol) of 1 M sodium borohydride ($NaBH_4$) stock solution in deionized water was added in two aliquots of 50 μL with vigorous stirring. For 5 and 10 nm AuNPs, we used the same method as the 1.5 nm AuNPs except for a smaller amount of ligand concentration. Following addition of the reducing agent, the color of the reaction mixture immediately became light brown for 1.5 nm AuNPs and orange-red for the 5 and 10 nm AuNPs. The mixture was then left stirring for at least 3 h. The AuNP dispersions were then purified from free ligands by three cycles of centrifugation using a membrane filtration device (10−30 kDa molecular weight cutoff, Millipore Corporation, Billerica, MA). NP concentration was determined as described previously.[39,43,45] The final NP sizes were confirmed by TEM measurement.

Synthesis of 20−100 nm AuNPs and Ligand Exchange with TA-NTA. AuNPs in the 20 to 100 nm size range were synthesized directly in aqueous phase by using a seeded growth method in the presence of citric acid and ascorbic acid. First 10 nm seed NPs were synthesized with sodium citrate and $NaBH_4$. The growth solution was prepared with 0.4 mM $HAuCl_4$ and 0.8 mM sodium citrate in 50 mL of deionized water. The desired amount of seed NPs, calculated based on the target size of AuNPs and seed size, was added to the growth solution followed by addition of L-ascorbic acid (2 mM final concentration). The reaction mixture was stirred for 3 h at room temperature and kept without stirring for an additional 24 h for the complete reaction. Reaction completion was confirmed by the red shift of the AuNP surface plasmon band peak and the corresponding decrease of the ascorbic acid and

DOI: 10.1021/acs.bioconjchem.9b00362
Bioconjugate Chem. 2019, 30, 2060−2074

aurate peaks in the near UV region (<300 nm) using UV−vis absorption spectroscopy. The final sizes were confirmed by TEM measurement.

For ligand exchange, the pre-synthesized larger AuNPs were added to an excess TA-NTA/TA mixture.[43] Briefly, 10 mL of as-synthesized citrate-modified AuNPs were mixed with an excess amount of mixed ligand stock solution (25, 10, and 5 μL of 100 mM stock for the 20, 55, and 100 nm AuNPs, respectively) containing 50% TA and 50% TA-NTA, which had been deprotected from the ester derivative with an equivalent molar concentration of NaOH for an hour before being mixed with TA. The solution was stirred for 8 h, adjusted to pH 8 by adding NaOH, and the dispersion was purified from free ligands by three cycles of centrifugation using a membrane filtration device.

Ni^{2+} Ion Coordination to NTA Ligands on AuNPs. AuNPs were loaded with Ni^{2+} for metal affinity coordination using a cation exchange column-based procedure. Briefly, the cation exchange column (10 cm length × 1 cm diameter) was prepared using CM Ion Exchange Chromatography Resin (Bio-Rad) and saturated with a 0.1 M $NiCl_2$ stock solution in water. The as-prepared NTA-modified AuNPs were added to the top of the CM column and kept in the column for at least 30 min to promote the interaction between the Ni^{2+} and NTA on the AuNP surface. The Ni^{2+}-NTA-modified AuNPs were eluted from the column using deionized water. The NP eluent was concentrated using a centrifugal membrane filter.

Phosphotriesterase and Assembly of AuNP-PTE Bioconjugates. PTE preparation has been previously described in detail.[33,36,49,54,63,75,76] Enzyme-to-NP ratios were controlled by matching the specific molar concentration of protein added to each of the AuNPs. AuNP-PTE bioconjugate formation was confirmed by separation using agarose gel electrophoresis. Preformed AuNP-PTE conjugates were loaded into wells of a 1% low electroendosmosis agarose gel supplemented with 1× TBE buffer (89 mM Tris-borate and 2 mM EDTA, pH 8.3). A potential of 95 V was then applied and the negatively charged AuNP-PTE conjugates migrated toward the anode. Images were taken ca. every 5 min on a Bio-Rad ChemiDoc Molecular Imager to visually monitor the differential changes in AuNP conjugate electrophoretic mobility in response to bioconjugation ratio.

Experiments were also undertaken to confirm that PTE did indeed attach to the AuNP series at both low and high coverage density with good efficiency. For this, samples across the AuNP series were allowed to form in an overnight reaction with PTE enzyme concentrations that matched both different reaction ratios of high and low coverage. Any remaining free-PTE in these samples was separated from the AuNP-PTE conjugates in the reaction using centrifuge dialysis filtration (100 kDa molecular weight cutoff, Millipore). A Bradford protein assay was then used to measure the amount of free-PTE removed from the reaction solution and compared to a standard assay curve made of free-PTE stock solution ranging in concentration from 10 nM to 10 μM. Measurements were repeated at least 3 times and averaged values of PTE/AuNP are presented in Table 1.

Enzymatic Assays. *Fixed Enzyme Density Assay.* In an effort to examine the influence of NP curvature on enzyme activity, we performed experiments in which NP size was varied while attempting to maintain the degree of enzyme coverage constant; see Figure 1B-bottom. This was achieved by varying AuNP concentration while holding the total concentration of enzyme fixed at 1.1 nM. The AuNP concentrations needed to keep the enzyme coverage unchanged were estimated by requiring that the PTE/AuNP ratio increase as the square of the AuNP diameter. Several different degrees of enzyme coverage (ca. 3−89%) were studied and these were achieved by varying the AuNP concentrations over the ranges indicated in parentheses: $AuNP_{5\ nm}$ (4.44 to 0.074 nM), $AuNP_{10\ nm}$ (1.11 to 0.019 nM), $AuNP_{20\ nm}$ (278 to 4.63 pM), and $AuNP_{55\ nm}$ (36.73 to 0.61 pM). For the 1.5 nm AuNPs, the ratio was varied from 0.5 to 3.0 PTE per AuNP and the $AuNP_{1.5\ nm}$ concentration was varied from 2.22 to 0.37 nM; these ratios are limited due to the small NP size as discussed below. For the 100 nm AuNP, the amount of AuNP needed for lower PTE:AuNP ratios became prohibitive, so the lower ratios were not performed; the final concentration of $AuNP_{100\ nm}$ was varied from 1.85 to 0.19 pM. Nickel-activated AuNPs were incubated in the presence of a stoichiometric amount of enzyme overnight at 4 °C at 0.1 μM PTE stock concentrations. The next day, 25 μL of each PTE:AuNP conjugate were diluted into wells of a 384-well plate to the final enzyme concentration of 1.1 nM. Immediately before measuring the absorbance, 25 μL of paraoxon substrate ranging in final concentration from 20 to 5000 μM was added to each well in a manner described previously.[36,48] Product formation of *p*-nitrophenol (pNP) was measured over time using a Tecan plate reader and a kinetic program in which the absorbance at 405 nm was measured every 25 s for no longer than 2 h. Net absorbance values were converted to pNP concentration using a standard curve for pNP ranging in concentration from 19.5 μM to 5 mM. The linear portions of the progress curves of pNP production were used to calculate the initial enzymatic rates as described previously.[36,48]

Fixed NP Diameter Assay. In an alternative assay format, the AuNP size was kept fixed and the PTE:NP ratio varied as shown in Figure 1B-bottom. This was achieved in our experiments by varying the AuNP concentration and keeping the total PTE concentration constant to achieve varying ratios of PTE per fixed size NP (see SI Table S3). The volume of 100 nm AuNPs needed to achieve the appropriate ratios was prohibitive; therefore, these experiments were not performed. Given the small size of the 1.5 nm AuNP, the concentration was varied from 0.28 to 2.78 nM. Based on the 10-nm-diameter AuNP size, the PTE/AuNP ratio was varied from 1 to 32 and this ratio set formed the basis for the ratios utilized with the other sizes of AuNP. Product formation was measured as described above.

Temperature and Viscosity Dependence. The influence of temperature on enzyme kinetics and enzyme activation energy was explored using an Arrhenius analysis as described previously.[36] The temperature was varied stepwise from 22 to 42 °C using the Tecan's temperature controls. PTE-product release rate was probed by including varying concentrations of sucrose so as to increase the assay viscosity as described previously.[36,50,62]

PTE Kinetic Analysis. The most common approach for analyzing enzyme kinetics is based on the Michaelis−Menten (MM) model in which the reaction steps are typically described as[60]

$$E + S \underset{k_{-1}}{\overset{k_1}{\rightleftarrows}} ES \xrightarrow{k_{cat}} E + P \tag{2}$$

Here, *E*, *S*, *P*, and *ES* correspond to the enzyme, substrate, product, and enzyme−substrate complex, respectively. Assum-

DOI: 10.1021/acs.bioconjchem.9b00362
Bioconjugate Chem. 2019, 30, 2060−2074

ing the kinetics are linear with the reaction constants as indicated in eq 2, the initial reaction velocity expression can be obtained as

$$V \cong \frac{k_{cat}e_0s_0}{K_M + s_0}\ (i) \qquad \text{where } K_M = \frac{k_{-1} + k_{cat}}{k_1}\ (ii) \tag{3}$$

Here, e_0 and s_0 represent the fixed enzyme and initial substrate concentrations, respectively (with both quantities being defined per unit total volume). At high substrate concentrations, the reaction velocity will reach its maximum, which according to eq 3*i* is $V_{max} = k_{cat}e_0$. Equation 3 typically fits the initial rate data well (e.g., Figure 3A,C); however, this does not necessarily validate the underlying MM model. Nevertheless, the experimentally derived regression parameters $\hat{k}_{cat}$ and $\hat{K}_M$, where the hats (not always included below when there is no ambiguity) emphasize that these are experimental values and not necessarily the theoretical MM ones of eq 2, can still serve as useful quantities for summarizing and comparing experimental data.

The hydrolysis of phosphotriesters by PTE has been studied in detail by the Raushel Lab,[50−53] and they suggest that a more realistic representation of the reaction mechanism(s) is[62]

$$E + S \underset{k_{-1}}{\overset{k_1}{\rightleftarrows}} ES \xrightarrow{k_{cat}^R} EP \underset{k_{-2}}{\overset{k_2}{\rightleftarrows}} E + P \tag{4}$$

where *EP* represents the enzyme−product complex. The modified MM reaction scheme of eq 4 differs in that the joint catalysis step is made more explicit by splitting into a "chemical" hydrolytic step (k_{cat}^R) and a "physical" product release step (k_2 and k_{-2}). This expanded version of the MM reaction is utilized as the basis for discussing the results. When k_{-2} can be neglected, the initial turnover rate in the MM kinetics obeys

$$V \cong \frac{k_{cat}e_0s_0}{K_M + s_0}\ (i) \qquad \text{where } k_{cat} \equiv \frac{k_{cat}^R k_2}{k_{cat}^R + k_2}\ (ii)$$
$$\text{and } \frac{K_M}{k_{cat}} \equiv \frac{K_M^R}{k_{cat}^R}\ (iii) \tag{5}$$

where $K_M^R = (k_{-1} + k_{cat}^R)/k_1$. That the functional form in eq 5(*i*) is identical to that of MM theory in eq 3(*i*) means that the same regression parameters derived from experiment, i.e., $\hat{k}_{cat}$ and $\hat{K}_M$, can be reinterpreted in terms of the modified MM model in eq 5. Fitting of the initial rate data, extrapolation of kinetic values, and other similar analyses were performed using the above formalism as previously described.[32,33,36]

■ ASSOCIATED CONTENT

Supporting Information

The Supporting Information is available free of charge on the ACS Publications website at DOI: 10.1021/acs.bioconjchem.9b00362.

Additional methods and experimental results (PDF)

■ AUTHOR INFORMATION

Corresponding Author

*E-mail: Igor.medintz@nrl.navy.mil.

ORCID

Eunkeu Oh: 0000-0003-1641-522X

Kimihiro Susumu: 0000-0003-4389-2574

Scott A. Walper: 0000-0002-9436-3456

Igor L. Medintz: 0000-0002-8902-4687

Author Contributions

#Equal contributions from Joyce C. Breger and Eunkeu Oh.

Notes

The authors declare no competing financial interest.

■ ACKNOWLEDGMENTS

The authors acknowledge ONR, NRL, and the NRL Nanoscience Institute for funding support, and the AIMLab in University of Maryland for assistance with TEM measurement. ILM also acknowledges the National Institute of Food and Agriculture, U.S. Department of Agriculture, under award number 11901762 for funding support.

■ REFERENCES

(1) Adrio, J. L., and Demain, A. L. (2014) Microbial Enzymes: Tools for Biotechnological Processes. *Biomolecules 4*, 117−139.

(2) National Academy of Science (2015) *Industrialization of Biology: A Roadmap To Accelerate the Advanced Manufacturing of Chemicals*, National Academies Press, Washington, D.C..

(3) DiCosimo, R., McAuliffe, J., Poulose, A. J., and Bohlmann, G. (2013) Industrial Use of Immobilized Enzymes. *Chem. Soc. Rev. 42*, 6437−6474.

(4) Franssen, M. C. R., Steunenberg, P., Scott, E. L., Zuilhof, H., and Sanders, J. P. M. (2013) Immobilised enzymes in biorenewables production. *Chem. Soc. Rev. 42*, 6491−6533.

(5) van der Helm, E., Genee, H. J., and Sommer, M. O. A. (2018) The Evolving Interface between Synthetic Biology and Functional Metagenomics. *Nat. Chem. Biol. 14*, 752−759.

(6) Woolston, B. M., Edgar, S., and Stephanopoulos, G. (2013) Metabolic Engineering: Past and Future. *Annu. Rev. Chem. Biomol. Eng. 4*, 259−288.

(7) Nielsen, J., and Keasling, J. D. (2016) Engineering Cellular Metabolism. *Cell 164*, 1185−1197.

(8) Dudley, Q. M., Karim, A. S., and Jewett, M. C. (2015) Cell-Free Metabolic Engineering: Biomanufacturing Beyond the Cell. *Biotechnol. J. 10*, 69−82.

(9) Rabe, K. S., Muller, J., Skoupi, M., and Niemeyer, C. M. (2017) Cascades in Compartments: En Route to Machine-Assisted Biotechnology. *Angew. Chem., Int. Ed. 56*, 13574−13589.

(10) Schrittwieser, J. H., Velikogne, S., Hall, M., and Kroutil, W. (2018) Artificial Biocatalytic Linear Cascades for Preparation of Organic Molecules. *Chem. Rev. 118*, 270−348.

(11) Guo, W. H., Sheng, J. Y., and Feng, X. Y. (2017) Mini-review: In vitro Metabolic Engineering for Biomanufacturing of High-value Products. *Comput. Struct. Biotechnol. J. 15*, 161−167.

(12) Opgenorth, P. H., Korman, T. P., and Bowie, J. U. (2014) A Synthetic Biochemistry Molecular Purge Valve Module that Maintains Redox Balance. *Nat. Commun. 5*, 4113.

(13) Kim, H., Sun, Q., Liu, F., Tsai, S. L., and Chen, W. (2012) Biologically Assembled Nanobiocatalysts. *Top. Catal. 55*, 1138−1145.

(14) Idan, O., and Hess, H. (2013) Origins of Activity Enhancement in Enzyme Cascades on Scaffolds. *ACS Nano 7*, 8658−8665.

(15) Idan, O., and Hess, H. (2013) Engineering Enzymatic Cascades on Nanoscale Scaffolds. *Curr. Opin. Biotechnol. 24*, 606−611.

(16) Karig, D. K. (2017) Cell-free Synthetic Biology for Environmental Sensing and Remediation. *Curr. Opin. Biotechnol. 45*, 69−75.

(17) Chen, W.-H., Vazquez-Gonzalez, V., Zoabi, A., Abu-Reziq, R., and Willner, I. (2018) Biocatalytic Cascades Driven By Enzymes Encapsulated in Metal−Organic Framework Nanoparticles. *Nat. Catalysis 1*, 689−695.

(18) Ansari, S. A., and Husain, Q. (2012) Potential Applications of Enzymes Immobilized on/in Nano Materials: A Review. *Biotechnol. Adv. 30*, 512−523.

(19) Ding, S. W., Cargill, A. A., Medintz, I. L., and Claussen, J. C. (2015) Increasing the Activity of Immobilized Enzymes with Nanoparticle Conjugation. *Curr. Opin. Biotechnol. 34*, 242−250.

DOI: 10.1021/acs.bioconjchem.9b00362
Bioconjugate Chem. 2019, 30, 2060−2074

(20) Vranish, J. N., Ancona, M. G., Walper, S. A., and Medintz, I. L. (2018) Pursuing the Promise of Enzymatic Enhancement with Nanoparticle Assemblies. *Langmuir 34*, 2901−2925.
(21) Johnson, B. J., Algar, W. R., Malanoski, A. P., Ancona, M. G., and Medintz, I. L. (2014) Understanding Enzymatic Acceleration at Nanoparticle Interfaces: Approaches and Challenges. *Nano Today 9*, 102−131.
(22) Patel, A. N., Anne, A., Chovin, A., Demaille, C., Grelet, E., Michon, T., and Taofifenua, C. (2017) Scaffolding of Enzymes on Virus Nanoarrays: Effects of Confinement and Virus Organization on Biocatalysis. *Small 13*, 1603163.
(23) Borhani, M. S., Etemadifar, Z., and Emtiazi, G. (2016) Enhancement of Production and Activity of Alkaline Zinc Metalloprotease from *Salinivibrio proteolyticus* Using Low Intensity Direct Electric Current and Zinc Nanoparticles. *Biotechnol. Lett. 38*, 1565−1570.
(24) Tsai, S. L., Park, M., and Chen, W. (2013) Size-Modulated Synergy of Cellulase Clustering for Enhanced Cellulose Hydrolysis. *Biotechnol. J. 8*, 257−261.
(25) Brown, C. W., Oh, E., Hastman, D. A., Walper, S. A., Susumu, K., Stewart, M. H., Deschamps, J. R., and Medintz, I. L. (2015) Kinetic Enhancement of the Diffusion-Limited Enzyme Beta-Galactosidase When Displayed with Quantum Dots. *RSC Adv. 5*, 93089−93094.
(26) Kouassi, G. K., Irudayaraj, J., and McCarty, G. (2005) Examination of Cholesterol oxidase attachment to magnetic nanoparticles. *J. Nanobiotechnol. 3*, 1.
(27) Holdrich, M., Sievers-Engler, A., and Lammerhofer, M. (2016) Gold Nanoparticle-Conjugated Pepsin for Efficient Solution-like Heterogeneous Biocatalysis in Analytical Sample Preparation Protocols. *Anal. Bioanal. Chem. 408*, 5415−5427.
(28) Medintz, I. (2006) Universal Tools for Biomolecular Attachment to Surfaces. *Nat. Mater. 5*, 842−842.
(29) Sapsford, K. E., Algar, W. R., Berti, L., Gemmill, K. B., Casey, B. J., Oh, E., Stewart, M. H., and Medintz, I. L. (2013) Functionalizing Nanoparticles with Biological Molecules: Developing Chemistries that Facilitate Nanotechnology. *Chem. Rev. 113*, 1904−2074.
(30) Ardao, I., Comenge, J., Benaiges, M. D., Alvaro, G., and Puntes, V. F. (2012) Rational Nanoconjugation Improves Biocatalytic Performance of Enzymes: Aldol Addition Catalyzed by Immobilized Rhamnulose-1-Phosphate Aldolase. *Langmuir 28*, 6461−6467.
(31) Campbell, A. S., Dong, C., Meng, F., Hardinger, J., Perhinschi, G., Wu, N., and Dinu, C. Z. (2014) Enzyme Catalytic Efficiency: A Function of Bio-Nano Interface Reactions. *ACS Appl. Mater. Interfaces 6*, 5393−5403.
(32) Vranish, J. N., Ancona, M. G., Oh, E., Susumu, K., and Medintz, I. L. (2017) Enhancing Coupled Enzymatic Activity by Conjugating One Enzyme to a Nanoparticle. *Nanoscale 9*, 5172−5187.
(33) Vranish, J. N., Ancona, M. G., Oh, E., Susumu, K., Lasarte-Aragones, G., Breger, J. C., Walper, S. A., and Medintz, I. L. (2018) Enhancing Coupled Enzymatic Activity by Colocalization on Nanoparticle Surfaces: Kinetic Evidence for Directed Channeling of Intermediates. *ACS Nano 12*, 7911−7926.
(34) Mukai, C., Gao, L. Z., Nelson, J. L., Lata, J. P., Cohen, R., Wu, L. R., Hinchman, M. M., Bergkvist, M., Sherwood, R. W., Zhang, S., et al. (2017) Biomimicry Promotes the Efficiency of a 10-Step Sequential Enzymatic Reaction on Nanoparticles, Converting Glucose to Lactate. *Angew. Chem., Int. Ed. 56*, 235−238.
(35) Sapsford, K. E., Tyner, K. M., Dair, B. J., Deschamps, J. R., and Medintz, I. L. (2011) Analyzing Nanomaterial Bioconjugates: A Review of Current and Emerging Purification and Characterization Techniques. *Anal. Chem. 83*, 4453−4488.
(36) Breger, J. C., Ancona, M. G., Walper, S. A., Oh, E., Susumu, K., Stewart, M. H., Deschamps, J. R., and Medintz, I. L. (2015) Understanding How Nanoparticle Attachment Enhances Phosphotriesterase Kinetic Efficiency. *ACS Nano 9*, 8491−8503.
(37) Oh, E., Huston, A. L., Shabaev, A., Efros, A., Currie, M., Susumu, K., Bussmann, K., Goswami, R., Fatemi, F. K., and Medintz, I. L. (2016) Energy Transfer Sensitization of Luminescent Gold Nanoclusters: More than Just the Classical Forster Mechanism. *Sci. Rep. 6*, 35538.
(38) Oh, E., Susumu, K., Blanco-Canosa, J. B., Medintz, I. L., Dawson, P. E., and Mattoussi, H. (2010) Preparation of Stable Maleimide-Functionalized Au Nanoparticles and Their Use in Counting Surface Ligands. *Small 6*, 1273−1278.
(39) Oh, E., Delehanty, J. B., Field, L. D., Makinen, A. J., Goswami, R., Huston, A. L., and Medintz, I. L. (2016) Synthesis and Characterization of PEGylated Luminescent Gold Nanoclusters Doped with Silver and Other Metals. *Chem. Mater. 28*, 8676−8688.
(40) Oh, E., Fatemi, F. K., Currie, M., Delehanty, J. B., Pons, T., Fragola, A., Leveque-Fort, S., Goswami, R., Susumu, K., Huston, A. L., et al. (2013) PEGylated Luminescent Gold Nanoclusters: Synthesis, Characterization, Bioconjugation, and Application to One- and Two-Photon Cellular Imaging. *Part. Part. Syst. Charact. 30*, 453−466.
(41) Diaz, S. A., Hastman, D. A., Medintz, I. L., and Oh, E. (2017) Understanding Energy Transfer with Luminescent Gold Nanoclusters: A Promising New Transduction Modality for Biorelated Applications. *J. Mater. Chem. B 5*, 7907−7926.
(42) Yu, H. Z., Rao, B., Jiang, W., Yang, S., and Zhu, M. Z. (2019) The Photoluminescent Metal Nanoclusters with Atomic Precision. *Coord. Chem. Rev. 378*, 595−617.
(43) Oh, E., Delehanty, J. B., Sapsford, K. E., Susumu, K., Goswami, R., Blanco-Canosa, J. B., Dawson, P. E., Granek, J., Shoff, M., Zhang, Q., et al. (2011) Cellular Uptake and Fate of PEGylated Gold Nanoparticles is Dependent on Both Cell-Penetration Peptides and Particle Size. *ACS Nano 5*, 6434−6448.
(44) Bilal, M., Oh, E., Liu, R., Breger, J. C., Medintz, I. L., and Cohen, Y. (2019) Bayesian Network Resource for Meta-Analysis: Cellular Toxicity of Quantum Dots. *Small*, 1900510.
(45) Oh, E., Susumu, K., Goswami, R., and Mattoussi, H. (2010) One-Phase Synthesis of Water-Soluble Gold Nanoparticles with Control over Size and Surface Functionalities. *Langmuir 26*, 7604−7613.
(46) Blanco-Canosa, J. B., Wu, M., Susumu, K., Petryayeva, E., Jennings, T. L., Dawson, P. E., Algar, W. R., and Medintz, I. L. (2014) Recent Progress in the Bioconjugation of Quantum Dots. *Coord. Chem. Rev. 263*, 101−137.
(47) *Chemoselective and Bioorthogonal Ligation Reactions: Concepts and Applications* (Algar, W. R., Dawson, P. E., and Medintz, I. L., Eds.) (2017) Wiley VCH.
(48) Diaz, S. A., Breger, J. C., and Medintz, I. L. Monitoring Enzymatic Proteolysis Using Either Enzyme- or Substrate-Bioconjugated Quantum Dots. In *Rational Design of Enzyme-Nanomaterials*; Methods in Enzymology Series; Elsevier, 2016; Vol. *571* , pp 19−54.
(49) Hondred, J. A., Breger, J. C., Garland, N. T., Oh, E., Susumu, K., Walper, S. A., Medintz, I. L., and Claussen, J. C. (2017) Enhanced Enzyme Activity of Phosphotriesterase Trimer Conjugated on Gold Nanoparticles for Pesticide Detection. *Analyst 142*, 3261−3271.
(50) Tsai, P. C., Bigley, A., Li, Y. C., Ghanem, E., Cadieux, C. L., Kasten, S. A., Reeves, T. E., Cerasoli, D. M., and Raushel, F. M. (2010) Stereoselective Hydrolysis of Organophosphate Nerve Agents by the Bacterial Phosphotriesterase. *Biochemistry 49*, 7978−7987.
(51) Bigley, A. N., and Raushel, F. M. (2013) Catalytic Mechanisms for Phosphotriesterases. *Biochim. Biophys. Acta, Proteins Proteomics 1834*, 443−453.
(52) Tsai, P. C., Fox, N., Bigley, A. N., Harvey, S. P., Barondeau, D. P., and Raushel, F. M. (2012) Enzymes for the Homeland Defense: Optimizing Phosphotriesterase for the Hydrolysis of Organophosphate Nerve Agents. *Biochemistry 51*, 6463−6475.
(53) Bigley, A. N., Xu, C. F., Henderson, T. J., Harvey, S. P., and Raushel, F. M. (2013) Enzymatic Neutralization of the Chemical Warfare Agent VX: Evolution of Phosphotriesterase for Phosphorothiolate Hydrolysis. *J. Am. Chem. Soc. 135*, 10426−10432.
(54) Breger, J. C., Walper, S. A., Oh, E., Susumu, K., Stewart, M. H., Deschamps, J. R., and Medintz, I. L. (2015) Quantum Dot Display Enhances Activity of a Phosphotriesterase Trimer. *Chem. Commun. 51*, 6403−6406.

DOI: 10.1021/acs.bioconjchem.9b00362
Bioconjugate Chem. 2019, 30, 2060−2074

(55) Susumu, K., Oh, E., Delehanty, J. B., Pinaud, F., Gemmill, K. B., Walper, S., Breger, J., Schroeder, M. J., Stewart, M. H., Jain, V., Whitaker, C. M., et al. (2014) A New Family of Pyridine-Appended Multidentate Polymers as Hydrophilic Surface Ligands for Preparing Stable Biocompatible Quantum Dots. *Chem. Mater. 26*, 5327−5344.
(56) Nieba, L., Nieba-Axmann, S. E., Persson, A., Hamalainen, M., Edebratt, F., Hansson, A., Lidholm, J., Magnusson, K., Karlsson, A. F., and Pluckthun, A. (1997) BIACORE Analysis of Histidine-tagged Proteins Using a Chelating NTA Sensor Chip. *Anal. Biochem. 252*, 217−228.
(57) Brown, C. W., Samanta, A., Diaz, S. A., Buckhout-White, S., Walper, S. A., Goldman, E. R., and Medintz, I. L. (2017) Dendrimeric DNA Nanostructures as Scaffolds for Efficient Bidirectional BRET-FRET Cascades. *Adv. Opt. Mater. 5*, 1700181.
(58) Lu, Y., Wang, J. P., Wang, J. H., Wang, L., Au, S. W. N., and Xia, J. (2012) Genetically Encodable Design of Ligand "Bundling" on the Surface of Nanoparticles. *Langmuir 28*, 13788−13792.
(59) Breger, J. C., Muttenthaler, M., Delehanty, J. B., Thompson, D. A., Oh, E., Susumu, K., Deschamps, J. R., Anderson, G. P., Field, L. D., Walper, S. A., et al. (2017) Nanoparticle Cellular Uptake by Dendritic Wedge Peptides: Achieving Single Peptide Facilitated Delivery. *Nanoscale 9*, 10447−10464.
(60) Cornish-Bowden, A. (2012) *Fundamentals of Enzyme Kinetics*, 4th ed., Wiley-Blackwell, Weinheim, Germany.
(61) Selwyn, M. J. (1965) A Simple Test for Inactivation of an Enzyme During Assay. *Biochim. Biophys. Acta, Enzymol. Biol. Oxid. 105*, 193−195.
(62) Caldwell, S. R., Newcomb, J. R., Schlecht, K. A., and Raushel, F. M. (1991) Limits of Diffusion in the Hydrolysis of Substrates by the Phosphotriesterase from *Pseudomonas diminuta*. *Biochemistry 30*, 7438−7444.
(63) Breger, J. C., Buckhout-White, S., Walper, S. A., Oh, E., Susumu, K., Ancona, M. G., and Medintz, I. L. (2017) Assembling High Activity Phosphotriesterase Composites Using Hybrid Nanoparticle Peptide-DNA Scaffolded Architectures. *Nano Futures 1*, 011002.
(64) Liu, Q., Wang, H., Shi, X. H., Wang, Z. G., and Ding, B. Q. (2017) Self-Assembled DNA/Peptide-Based Nanoparticle Exhibiting Synergistic Enzymatic Activity. *ACS Nano 11*, 7251−7258.
(65) Giust, D., Lucio, M. I., El-Sagheer, A. H., Brown, T., Williams, L. E., Muskens, O. L., and Kanaras, A. G. (2018) Graphene Oxide-Upconversion Nanoparticle Based Portable Sensors for Assessing Nutritional Deficiencies in Crops. *ACS Nano 12*, 6273−6279.
(66) Kyriazi, M. E., Giust, D., El-Sagheer, A. H., Lackie, P. M., Muskens, O. L., Brown, T., and Kanaras, A. G. (2018) Multiplexed mRNA Sensing and Combinatorial-Targeted Drug Delivery Using DNA-Gold Nanoparticle Dimers. *ACS Nano 12*, 3333−3340.
(67) Zobel, M., Neder, R. B., and Kimber, S. A. J. (2015) Universal Solvent Restructuring Induced by Colloidal Nanoparticles. *Science 347*, 292−294.
(68) Pfeiffer, C., Rehbock, C., Huhn, D., Carrillo-Carrion, C., de Aberasturi, D. J., Merk, V., Barcikowski, S., and Parak, W. J. (2014) Interaction of Colloidal Nanoparticles with Their Local Environment: The (Ionic) Nanoenvironment Around Nanoparticles is Different from Bulk and Determines the Physico-Chemical Properties of the Nanoparticles. *J. R. Soc., Interface 11*, 20130931.
(69) Claussen, J. C., Malanoski, A., Breger, J. C., Oh, E., Walper, S. A., Susumu, K., Goswami, R., Deschamps, J. R., and Medintz, I. L. (2015) Probing the Enzymatic Activity of Alkaline Phosphatase within Quantum Dot Bioconjugates. *J. Phys. Chem. C 119*, 2208−2221.
(70) Lata, J. P., Gao, L. Z., Mukai, C., Cohen, R., Nelson, J. L., Anguish, L., Coonrod, S., and Travis, A. J. (2015) Effects of Nanoparticle Size on Multilayer Formation and Kinetics of Tethered Enzymes. *Bioconjugate Chem. 26*, 1931−1938.
(71) Castellana, M., Wilson, M. Z., Xu, Y. F., Joshi, P., Cristea, I. M., Rabinowitz, J. D., Gitai, Z., and Wingreen, N. S. (2014) Enzyme Clustering Accelerates Processing of Intermediates Through Metabolic Channeling. *Nat. Biotechnol. 32*, 1011−1018.
(72) Wheeldon, I., Minteer, S. D., Banta, S., Barton, S. C., Atanassov, P., and Sigman, M. (2016) Substrate Channelling as an Approach to Cascade Reactions. *Nat. Chem. 8*, 299−309.
(73) Schrittwieser, J. H., Velikogne, S., Hall, M., and Kroutil, W. (2018) Artificial Biocatalytic Linear Cascades for Preparation of Organic Molecules. *Chem. Rev. 118*, 270−348.
(74) Dwyer, C. L., Diaz, S. A., Walper, S. A., Samanta, A., Susumu, K., Oh, E., Buckhout-White, S., and Medintz, I. L. (2015) Chemoenzymatic Sensitization of DNA Photonic Wires Mediated through Quantum Dot Energy Transfer Relays. *Chem. Mater. 27*, 6490−6494.
(75) Alves, N. J., Moore, M., Johnson, B. J., Dean, S. N., Turner, K. B., Medintz, I. L., and Walper, S. A. (2018) Environmental Decontamination of a Chemical Warfare Simulant Utilizing a Membrane Vesicle-Encapsulated Phosphotriesterase. *ACS Appl. Mater. Interfaces 10*, 15712−15719.
(76) Alves, N. J., Turner, K. B., Daniele, M. A., Oh, E., Medintz, I. L., and Walper, S. A. (2015) Bacterial Nanobioreactors-Directing Enzyme Packaging into Bacterial Outer Membrane Vesicles. *ACS Appl. Mater. Interfaces 7*, 24963−24972.

DOI: 10.1021/acs.bioconjchem.9b00362
Bioconjugate Chem. 2019, 30, 2060−2074